Acta Pharmaceutica Sinica B 2024;14(10):4312–4328

Chinese Pharmaceutical Association
Institute of Materia Medica, Chinese Academy of Medical Sciences

Acta Pharmaceutica Sinica B

www.elsevier.com/locate/apsb
www.sciencedirect.com

ORIGINAL ARTICLE

Demethylzeylasteral induces PD-L1 ubiquitin–proteasome degradation and promotes antitumor immunity *via* targeting USP22

Yanyan Zhang [a,†], Yun Huang [a,†], Dianping Yu [a], Mengting Xu [a], Hongmei Hu [a], Qing Zhang [a], Minchen Cai [a], Xiangxin Geng [a], Hongwei Zhang [a], Jianhua Xia [a], Mengmeng Guo [a], Dong Lu [a], Hanchi Xu [a], Linyang Li [a], Xing Zhang [a], Qun Wang [a,*], Sanhong Liu [a,*], Weidong Zhang [a,b,c,d,*]

[a]*Shanghai Frontiers Science Center of TCM Chemical Biology, Institute of Interdisciplinary Integrative Medicine Research, Shanghai University of Traditional Chinese Medicine, Shanghai 201203, China*
[b]*Department of Phytochemistry, School of Pharmacy, Second Military Medical University, Shanghai 200433, China*
[c]*Institute of Medicinal Plant Development, Chinese Academy of Medical Sciences and Peking Union Medical College, Beijing 100193, China*
[d]*The Research Center for Traditional Chinese Medicine, Shanghai Institute of Infectious Diseases and Biosafety, Institute of Interdisciplinary Integrative Medicine Research, Shanghai University of Traditional Chinese Medicine, Shanghai 201203, China*

Received 30 April 2024; received in revised form 11 June 2024; accepted 25 July 2024

KEY WORDS

Demethylzeylasteral;
PD-L1;
USP22;
Deubiquitination;
Tumor-infiltrating lymphocytes;

Abstract Programmed cell death ligand-1 (PD-L1) is a T cell inhibitory immune checkpoint molecule that interacts with programmed cell death-1 (PD-1) to promote immune escape of tumor cells. Compared with antibody therapies, small molecule drugs show better prospects due to their advantages such as higher bioavailability, better tissue penetration, and reduced risk of immunogenicity. Here, we found that the small molecule demethylzeylasteral (Dem) can significantly downregulate the expression of PD-L1 in colorectal cancer cells and enhance the killing effect of T cells on tumor cells. Mechanistically, Dem binds to the deubiquitinating enzyme USP22 and promotes its degradation, resulting in increased

*Corresponding authors.
E-mail addresses: wdzhangy@hotmail.com (Weidong Zhang), liush@shutcm.edu.cn (Sanhong Liu), Qunwang0523@163.com (Qun Wang).
[†]These authors made equal contributions to this work.
Peer review under the responsibility of Chinese Pharmaceutical Association and Institute of Materia Medica, Chinese Academy of Medical Sciences.

https://doi.org/10.1016/j.apsb.2024.08.004

Colorectal cancer;
Immune checkpoint blockade;
Antitumor immunity

ubiquitination and degradation of PD-L1 through the proteasome pathway. In addition, Dem increased the activity of cytotoxic T cells and reduced the number of myeloid-derived suppressor cells (MDSCs) and regulatory T cells (Tregs) in tumor-infiltrating lymphocytes (TILs), thereby activating the tumor immune microenvironment and inhibiting the growth of subcutaneous MC38 tumors in C57BL/6 mice. Moreover, we also found that the combination of Dem and CTLA4 antibodies can further improve the efficacy of antitumor therapy. Our study reveals the mechanism by which Dem promotes PD-L1 degradation and suggests that the combination of Dem and CTLA4 antibodies may improve the efficacy of immunotherapy.

1. Introduction

Programmed death ligand-1 (PD-L1) is a T cell inhibitory checkpoint molecule that is constitutively expressed on the surface of cancer cells[1]. The interaction between PD-L1 and its receptors can inactivate tumor-infiltrating immune cells expressing cell surface programmed death-1 (PD-1; also known as CD279), causing cancer cells to evade immune surveillance[2,3]. Blockade of the PD-1/PD-L1 axis has attracted considerable attention as a potential target for cancer immunotherapy, and it has achieved impressive therapeutic results in patients with a variety of cancer types[4,5]. Although antibody therapy has achieved good therapeutic effects in clinical practice, many patients fail to obtain long-term clinical benefits because the expression of PD-L1 in tumor cells is complexly regulated. Since antibody treatment can only effectively inhibit the function of PD-L1 on the surface of tumor cells, the new PD-L1 synthesized from ribosomes is processed and modified by the endoplasmic reticulum and Golgi apparatus and then rapidly restores the expression of PD-L1 on the cell membrane through the endocytic cycle, greatly reducing the effect of antibody treatment[6-8]. Therefore, improving the efficacy of immune checkpoint blockade (ICB) therapy has become a current research hotspot.

Posttranslational modifications of PD-L1 include ubiquitination, glycosylation, phosphorylation, palmitoylation, acetylation, and SUMOylation, which play important roles in regulating PD-L1 stability[9]. Increasing evidence that PD-L1 is regulated by the ubiquitin-proteasome pathway suggests that targeting PD-L1 polyubiquitination is an alternative approach to enhance immune checkpoint therapy[10]. Ubiquitination refers to the process by which ubiquitin covalently binds and degrades target proteins catalyzed by a series of enzymes, in which the E3 ubiquitin ligase determines the specific recognition of target proteins[1,11]. Several E3 ligases, such as HRD1, BTRC, STUB1, ARIH1, SPOP, A20, and MARCH8, have been found to target PD-L1 for degradation under various physiological and pathological conditions[12-18].

Deubiquitination is the reverse process of ubiquitination mediated by deubiquitinating enzymes[11]. Ubiquitin-specific peptidase 22 (USP22) belongs to the ubiquitin-specific protease family of deubiquitinating enzymes. USP22 is a deubiquitinating enzyme of PD-L1 that can directly bind to the C-terminus of PD-L1, induce its deubiquitination, and stabilize its expression. Moreover, USP22 can bind to CSN5 to deubiquitinate it, inhibit its degradation, and ultimately prolong the half-life of PD-L1[19,20]. Clinically, USP22 is highly expressed in colorectal cancer (CRC), lung cancer, liver cancer, pancreatic cancer, and other cancers and is related to the poor prognosis of clinical patients[21-23]. Therefore, USP22 is a promising target for immune checkpoint therapy.

Demethylzeylasteral (Dem) is a triterpene compound extracted from the traditional Chinese medicine *Tripterygium wilfordii* Hook F that has a wide range of biological activities[24]. Studies have shown that Dem has anti-inflammatory and immunosuppressive effects. Furthermore, Dem also has a remarkable inhibitory impact on the growth of liver cancer, melanoma, glioma, and other types of cancer cells[25-27]. However, it remains unclear whether Dem, as an immunomodulator, has the potential to promote antitumor immunity.

In this study, we screened a compound library containing 225 small molecules (Supporting Information Table S1) from traditional Chinese medicine and found that Dem can significantly inhibit the expression of PD-L1 in colorectal cancer cells. Our mechanistic results suggest that Dem can block the deubiquitination of PD-L1 by binding to the deubiquitination enzyme USP22, thereby promoting the degradation of PD-L1 and activating antitumor immunity.

2. Materials and methods

2.1. Reagents

The antibodies used are listed in Supporting Information Table S2. MG132, Baf (bafilomycin), CQ (chloroquine), 3-MA (3-methyladenine), and CHX (cycloheximide) were purchased from MedChemExpress (Monmouth Junction, NJ, USA). Recombinant human IFN-γ was purchased from PeproTech (NJ, USA). 0.25% trypsin−EDTA, 5 × protein loading buffer, and protease inhibitor were obtained from Meilun Biotechnology (Dalian, China). The reverse transcription kit was purchased from Yeasen (Shanghai, China). Pronase was purchased from Roche (Basel, Switzerland). Demethylzeylasteral was obtained from Shanghai Sunny Biotech Co., Ltd. (Shanghai, China).

2.2. Cell lines and culture

Colorectal carcinoma (RKO and HT29) and lung carcinoma (A549) cells were obtained from the Cell Bank of Shanghai Institute of Cell Biology, Chinese Academy of Sciences (SIBS, CAS). Lung carcinoma cells (H460) were obtained from ATCC (Manassas, VA, USA). Jurkat cells were donated by the Kongming Wu research group (Department of Oncology, Tongji Hospital of

Tongji Medical College, Huazhong University of Science and Technology, Wuhan, China). RKO (a poorly differentiated colon carcinoma cell line and the parental cell line (isogenic) of RKO-E6 (ATCC CRL-2578) and RKO-A545-1 (ATCC CRL-2579)) were maintained in MEM supplemented with 10% FBS and NEAA (Meilun Biotechnology, Dalian, China). HT29 cells (isolated from a primary tumor in 1964 by J. Fogh using the explant culture method) were maintained in McCoy's 5A medium (Meilun Biotechnology, Dalian, China) supplemented with 10% FBS (Biological Industries, Cromwell, CT, USA). A549 cells (isolated from the lungs of a 58-year-old white male with carcinoma) and H460 cells (derived from the pleural fluid of a patient with large cell cancer of the lung by A.F. Gazdar and associates in 1982) were maintained in DMEM (Meilun Biotechnology, Dalian, China) supplemented with 10% FBS. Jurkat cells were maintained in RIPM 1640 (Meilun Biotechnology, Dalian, China) supplemented with 10% FBS.

2.3. Cell viability assay

Cell viability was explored with a Cell Counting Kit-8 (CCK-8) (APExBio, Houston, TX, USA). Cells were seeded at a density of 5×10^3 per well in 96-well plates and allowed to attach overnight. Then, the cells were treated with different concentrations of Dem for 24 h. These results were used to evaluate the effect of Dem on cell viability.

2.4. 5-Ethynyl-2′-deoxyuridine (EdU) assay

The 5-ethynyl-2′-deoxyuridine (EdU) assay was used to determine the effect of Dem on cell proliferation. Cells were seeded at a density of 2×10^5 per well in 12-well plates and allowed to attach overnight. Then, the cells were treated with different concentrations of Dem for 24 h. The proliferation of the cells was detected by an EdU assay kit (Beyotime, Haimen, China). The steps followed the product manual. All the cells were taken by using Operetta CLS (PerkinElmer, USA).

2.5. Western blotting analysis and immunoprecipitation

Cells were seeded at a density of 5×10^5 per well in 6-well plates. These cells were treated with or without Dem for 24 h. All the cells were collected for Western blotting analysis. Total cellular proteins were extracted with RIPA lysis buffer (Beyotime, Haimen, China). The protein concentrations were detected by using a BCA protein assay kit (Beyotime, Haimen, China). Twenty micrograms of protein were separated *via* 10% SDS−PAGE and electrotransferred onto PVDF membranes. After blocking in 5% nonfat milk for 1 h at room temperature, the membranes were incubated with the corresponding primary antibodies at 4 °C overnight and with horseradish peroxidase-conjugated secondary antibodies at room temperature for 1 h. The immunoreactive bands were scanned with an imaging system (Bio-Rad, USA).

For inhibitor experiments, cells were treated with Dem in the absence or presence of the proteasome inhibitor MG132 or the lysosome inhibitors Baf, CQ, and 3-MA. For CHX chase studies, cells were treated with Dem for 12 h, and 25 μg/mL CHX was added at the indicated time points. The subsequent processing was consistent with the above procedure.

For immunoprecipitation, the cells were treated with Dem (10 μmol/L) in the presence of MG132. The lysate was incubated overnight with IgG or an anti-PD-L1 antibody at 4 °C with rotation. Then, protein A/G beads (Santa Cruz Biotechnology, USA) were added, and the mixture was incubated at 4 °C for 3 h with rotation. After that, the protein A/G beads were rinsed five times with IP lysis solution, and the samples were analyzed by immunoblotting.

2.6. RNA extraction and real-time PCR analysis

Total RNA was isolated from the transferred cells using RNAiso Plus (Takara, Shiga, Japan). Total mRNA (1 μg) was reverse transcribed into cDNA using the Prime Script RT reagent Kit (Takara, Shiga, Japan) according to the manufacturer's instructions. Quantitative RT-PCR was performed using a LightCycler® 96 instrument (Roche, Basel, Switzerland). β-Actin or GAPDH was used as the reference gene. The sequences of the primers used are listed in Supporting Information Table S3.

2.7. Cell transfection for gene silencing and overexpression

The siRNAs for PD-L1, USP22, HRD1, BTRC, STUB1, ARIH1, SPOP, A20, and MARCH8 were purchased from GenePharma (Shanghai, China), and the sequences used are listed in Supporting Information Table S4. A negative control (NC) was used as a control. RKO cells were seeded at 2×10^5 per well in 6-well plates and cultured for 24 h. Then, these cells were transfected with siRNA duplexes by Lipofectamine 3000 (Invitrogen, Carlsbad, CA) and incubated for 48 h.

The pcDNA3.1-PD-L1, pcDNA3.1-Ub, pcDNA3.1-CSN5, pcDNA3.1-OTUB1, pcDNA3.1-USP22, and pcEGFP-USP22 plasmids were obtained from GenePharma (Shanghai, China). The USP22-Arg371 and USP22-His374 mutants were generated by site-directed mutagenesis PCR using platinum Pwo SuperYield DNA polymerase (NEB) according to the manufacturer's instructions. All the plasmids were sequenced to confirm whether the designed mutation was present without any other unwanted mutation. The rest of the steps were similar to those above.

2.8. Flow cytometry analysis of membrane PD-L1

For flow cytometric analysis of membrane PD-L1, RKO, HT29, A549, and H460 cells were treated with Dem for the indicated times in the absence or presence of IFN-γ (50 ng/mL). Then, the cells were collected and incubated with a PE-conjugated PD-L1 antibody at 4 °C for 30 min in the dark. After washing twice with PBS, the cells were analyzed using flow cytometry (Beckman Coulter Cytoflex, USA).

2.9. Immunofluorescence staining assay

The immunofluorescence staining assay was conducted as previously described[28]. RKO and HT29 cells were seeded at 2×10^5 per well in 12-well plates and treated with Dem for 24 h. After the supernatant was discarded, the cells were fixed with 4% formaldehyde and permeabilized with 0.5% Triton X-100. Then, the sections were blocked with 5% BSA for 1 h at room temperature. After that, the cells were incubated with a diluted primary antibody at 4 °C overnight and with a fluorescent-labeled secondary antibody at room temperature for 1 h. Finally, a DAPI-containing antifade mounting medium (Beyotime, Haimen, China) was added. The images were taken with a Cytation 5 (BioTek, USA).

For inhibitors, cells were treated with Dem in the absence or presence of the proteasome inhibitor MG132 or the lysosome inhibitor CQ. The subsequent processing was consistent with the above procedure.

2.10. T cell-mediated tumor cell killing assay

The T cell-mediated tumor cell killing assay was performed as described previously[29]. We used Jurkat cells stably transfected with human PD-1 to coculture with RKO and HT29 cells. RKO and HT29 cells were seeded at 3×10^5 per well in 12-well plates and treated with Dem for 24 h in the absence or presence of IFN-γ (50 ng/mL). Jurkat cells were activated by 1 mg/mL phytohemagglutinin (PHA) and 50 ng/mL phorbol 12-myristate 13-acetate (PMA). Then, the tumor cells were cocultured with activated T cells for 24 h at a ratio of 1:9 (for RKO or HT29 cells: T cells). After the cell debris and T cells were washed off with PBS, the remaining cells were fixed with 4% paraformaldehyde for 15 min and stained with crystal violet. These images were taken with a Cytation 5 (BioTek, USA).

2.11. Proteomic analysis

RKO cells were cultured in 10 cm culture dishes and incubated until the cell density reached 70%−80%. Afterward, the cells were treated with Dem (10 μmol/L) or an equal volume of DMSO for 24 h. Each sample was subjected to an SDT lysis procedure. According to the requirements of the process, all the samples were digested with trypsin at 37 °C for 16−18 h. The remaining steps were followed by LC−MS/MS.

2.12. Cellular thermal shift assay (CETSA)

The CETSA experiment was carried out as described previously[30]. RKO cells were collected and lysed in liquid nitrogen. After centrifugation, the supernatant was collected and divided into two equal parts. After that, the two lysates were incubated with Dem (100 μmol/L) or the solvent control (DMSO) for 5−10 min at room temperature. The samples were divided into 100 μL/tube volumes, heated at different temperatures (37, 48, 51, 54, 57, 60, 63, 66, 69, 72, and 75 °C) for 3 min, cooled at room temperature for 3 min and kept on ice. For concentration−response studies, cell lysate samples were incubated with Dem at specified concentrations, heated at room temperature for 3 min, cooled for 3 min at room temperature, and kept on ice. All the samples were centrifuged (only soluble fractions were collected), and the supernatants were analyzed *via* Western blotting.

2.13. Drug affinity responsive target stability (DARTS)

The DARTS assay was performed as previously described[31]. Briefly, different concentrations of Dem were added to an equal volume of RKO cell lysate and incubated at room temperature for 1 h. Then, the samples were digested with pronase at the specified ratios for 30 min at room temperature. After digestion, a loading buffer was added, and the samples were boiled and analyzed *via* Western blotting.

2.14. Molecular docking of Dem to USP22

The molecular structure of compound Dem was obtained from the PubChem database (https://pubchem.ncbi.nlm.nih.gov/) and imported into Molecular Operating Environment (MOE) software. The protonated 3D and energy minimization modules were used for protonation and energy minimization, respectively. The crystal structure of USP22 is not yet available, and its 3D structure was predicted and obtained using AlphaFold2 (https://alphafold.ebi.ac.uk/), which was imported into the MOE. Water molecules farther than 4.5 Å from the protein receptor were removed. Then, the protein structures were prepared by the QuickPrep tool in MOE with the default parameters, including structure preparation, protonation, and energy minimization. The SiteFinder module in the MOE was used to predict the potential small-molecule binding sites of USP22, and the DOCK module in the MOE was used for molecular docking calculations. The refinement method was set to induced fit, and the other parameters were set to their defaults. After the completion of the molecular docking calculation, the docking results with the highest score were selected to analyze the potential binding modes of the compounds Dem and USP22.

2.15. Microscale thermophoresis (MST)

The MST measurements for binding of Dem to USP22 were performed as described previously[32]. In brief, we expressed the GFP-carrying plasmid in 293T cells, and the lysates were collected after 48 h of transfection. The samples were analyzed by a MonolithTM NT.115 MST device (NanoTemper, Germany). Using nanoblue excitation, the LED light was adjusted to 45% excitation power, and the MST power was adjusted to medium. The software was used in Expert mode to allow thermophoresis and fluorescence detection for 30 s.

2.16. USP22 deubiquitinating activity assay

USP22 deubiquitinating activity assay was conducted in a 96-well plate in 100 μL of reaction buffer supplemented with Ub-7-amino-4-methylcoumarin (AMC)-conjugated proteins (U-550; Boston Biochem, Cambridge, MA, USA). AMC fluorescence was measured with an excitation wavelength of 345 nm and an emission wavelength of 445 nm.

2.17. Subcutaneous tumor model

All animal studies were approved by the Committee on the Ethics of Animal Experiments of the Shanghai University of Traditional Chinese Medicine (SHUTCM) and complied with national and international guidelines. Six-week-old female C57BL/6 mice and nude mice were purchased from Shanghai SLAC Laboratory Animal (Shanghai, China) and housed under specific pathogen-free conditions. For C57BL/6 mice, 8×10^5 MC38 cells were injected subcutaneously. When the average tumor volume reached approximately 50 mm^3, the mice were randomly divided into four groups. The treatment group was injected with 1, 2, or 4 mg/kg Dem daily for 12 days, and those in the control group were injected with the same volume of saline. Body weights and tumor sizes were recorded every two days.

Consistent with the above description, the nude mice were randomly divided into two groups: the Dem treatment group and the control group. The plants in the treatment group were injected with 4 mg/kg Dem daily for 10 days, and those in the control group were injected with the same volume of saline. Additionally, body weights and tumor sizes were recorded every two days.

For combination therapy with Dem and anti-CTLA4, as described above, the mice were randomly divided into seven treatment groups: control group (saline); anti-PD-L1 treatment group: anti-PD-L1 (100 μg/100 μL); anti-CTLA4 treatment group: anti-CTLA4 (100 μg/100 μL); Dem treatment group: Dem (4 mg/kg); Dem and anti-PD-L1 combination group: anti-PD-L1 (100 μg/100 μL) and Dem (4 mg/kg); Dem and anti-CTLA4

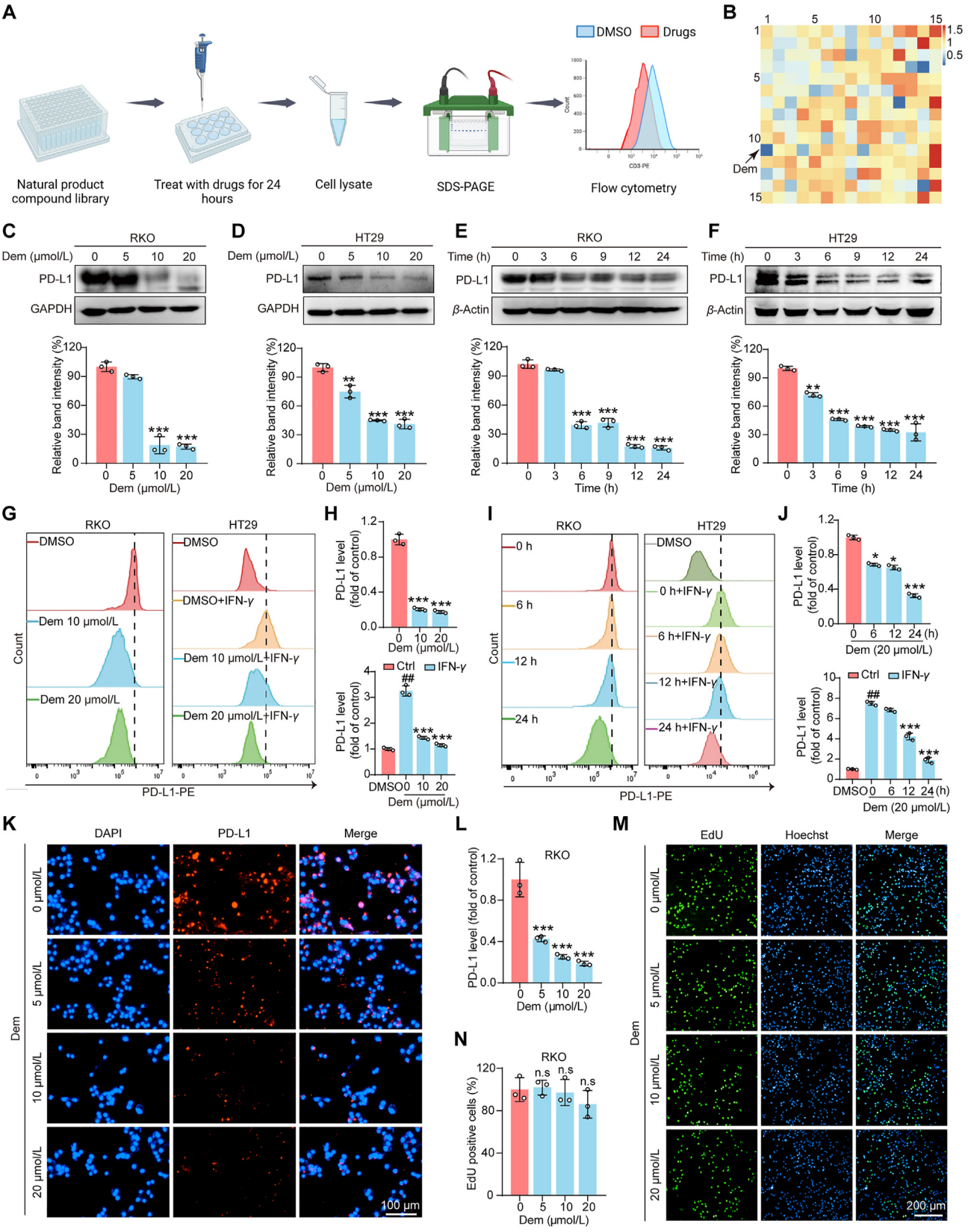

Figure 1 Dem can downregulate PD-L1 expression in CRC cells. (A) Process diagram of the screening of small molecules that can downregulate the expression of PD-L1 in RKO cells from the compound library. (B) A total of 225 molecules were screened in the compound library. RKO cells were treated with the drugs at 10 μmol/L for 24 h. The hit compounds that induced a decrease in PD-L1 levels are shown in blue. A depth of blue represents a decreased level of PD-L1. The reduction in PD-L1 levels in RKO cells treated with 225 drugs was measured *via* Western blotting. The corresponding small molecule names can be found in Supporting Information Table S1. (C, D) RKO and HT29 cells were

combination group: anti-CTLA4 (100 μg/100 μL) and Dem (4 mg/kg); anti-PD-L1 and anti-CTLA4 combination group: anti-PD-L1 (100 μg/100 μL) and anti-CTLA4 (100 μg/100 μL). When the average tumor volume reached approximately 50 mm^3, Dem was injected daily, and anti-PD-1 and anti-CTLA4 antibodies were administered every five days. Additionally, body weights and tumor sizes were recorded every two days.

Tumor size was calculated by using the following formula: volume (mm^3) = length × ($width^2$)/2. After completing the experiment, the mice were sacrificed, and the tumors and other major organs, such as the liver, spleen, kidney, and heart, were isolated and collected.

2.18. *Tumor-infiltrating lymphocyte isolation and T cell profile analysis*

Tumor-infiltrating lymphocyte isolation and T cell profile analysis were performed as described previously[29]. Tumor tissues from the mice were collected and cut into small pieces, and the samples were subsequently digested for 1 h at 37 °C with type 4 collagenase (1 mg/mL, Yeasen) and DNase 1 (0.1 mg/mL, Yeasen). Then, the cells were incubated with the surface-labeled antibodies against mouse CD25, CD3, CD8, Gr-1, CD11b, and Foxp3 for 30 min at 4 °C and finally stained with anti-mouse GzmB for 30 min. Data acquisition was performed by using flow cytometry (Beckman Coulter Cytoflex, USA).

2.19. *Immunohistochemistry (IHC) analysis*

For immunohistochemistry, tumor specimens were fixed with 4% paraformaldehyde and embedded in paraffin. Briefly, paraffin-embedded tissue sections were deparaffinized in xylene and treated with a series of graded alcohols and distilled water. The antigen was recovered by microwave boiling in 10 mmol/L sodium citrate buffer (pH 6.0) and incubating with 3% H_2O_2 to block endogenous peroxide activity. Then, 5 μm thick sections were stained for PD-L1 (1:200), Foxp3 (1:200), CD8 (1:200), c-caspase-3 (1:200), and Ki-67 (1:200) at 4 °C overnight. A horseradish peroxidase-conjugated secondary antibody (1:1000) and DAB were used for detection, and the slides were counterstained with hematoxylin. Images were captured with a Cytation 5 (BioTek, USA).

2.20. *Statistical analysis*

GraphPad Prism 8.0.1 was used to collect and analyze the data. ImageJ was used for grayscale quantification of protein bands and measurement of average fluorescence intensity. Statistical analysis was performed with an unpaired t-test when two different groups were compared or one-way ANOVA with Tukey's multiple comparison test. All calculated values are shown as the mean ± standard errors of the mean (SEM). All the statistical analyses were performed using SPSS software (version 16.0, SPSS, Chicago, IL, USA).

3. Results

3.1. *Dem is a potent negative modulator of PD-L1*

To identify small molecules that can reduce PD-L1 abundance in colorectal cells and exert immune-related antitumor effects, a compound library containing 225 small molecules from Chinese medicine was screened. First, RKO cells were incubated with the test compounds (10 μmol/L) for 24 h, after which the PD-L1 level was determined *via* Western blotting. Then, for small molecules that can significantly downregulate PD-L1 protein levels, flow cytometry further validated the effects of PD-L1 expression on the cell membrane (Fig. 1A). By screening 225 small molecule compounds, we found that three small molecules, namely, demethylzeylasteral (Supporting Information Fig. S1A), micheliolide and praeruptorin A, significantly reduced the expression of PD-L1 in RKO cells (Fig. 1B). Studies have shown that micheliolide can trigger ROS-mediated ERS-driven immunogenic cell death in hepatocellular carcinoma[33]. Consistent with our findings, although micheliolide significantly reduced the expression of PD-L1 in RKO cells, it also exhibited strong cytotoxicity (Fig. S1B). The results showed that praeruptorin A significantly reduced PD-L1 protein levels in RKO cells, while flow cytometry failed to detect a decrease in the expression of PD-L1 on the cell membrane (Fig. S1C), and only reduced PD-L1 expression in the cell membrane affected immunosuppressive function. Encouragingly, Dem at this concentration significantly reduced not only intracellular PD-L1 expression but also PD-L1 expression on the cell membrane with no visible cytotoxicity. Since we expected to obtain small molecules that have no significant cytotoxicity, can reduce the expression of PD-L1 on cancer cells, and have not yet been reported, Dem was chosen for subsequent experiments.

3.2. *Dem significantly downregulates PD-L1 expression in cancer cells*

We next further validated the effect of Dem on PD-L1 expression in colorectal cancer cells. We found that Dem induced significant dose- and time-dependent decreases in constitutive PD-L1 expression in RKO and HT29 cells (Fig. 1C−F). Therefore, 0−20 μmol/L Dem was used for subsequent experiments in this

treated with different concentrations of Dem for 24 h, after which total PD-L1 was analyzed by immunoblotting (IB). The results of the quantitative IB analysis are shown below. (E, F) RKO and HT29 cells were treated with Dem (10 or 20 μmol/L) for the indicated times and subjected to IB analysis of total PD-L1. The results of the quantitative IB analysis are shown below. (G) RKO and HT29 cells were treated with different concentrations of Dem for 24 h in the absence or presence of IFN-γ (50 ng/mL), and the plasma membrane PD-L1 concentration was detected *via* flow cytometry. (I) RKO and HT29 cells were treated with Dem for the indicated times in the absence or presence of IFN-γ (50 ng/mL), and the plasma membrane PD-L1 concentration was detected *via* flow cytometry. (H, J) Quantitative analysis of plasma membrane PD-L1 expression. $^{\#\#}P < 0.01$ compared with DMSO group; $^{***}P < 0.001$ compared with the IFN-γ DMSO group. (K) Immunofluorescence staining images of RKO cells. PD-L1 is labeled in red, and nuclei are labeled in blue with DAPI. Scale bar = 100 μm. (L) The quantitative results of immunofluorescence staining. (M) Images of EdU-stained cells showing the effect of Dem on RKO cell proliferation (represented by green fluorescence) and nuclei are labeled in blue with Hoechst. Scale bar = 200 μm. (N) The quantitative results of EdU staining. The data shown are the mean ± standard error of the mean (SEMs); $n = 3$; n.s $P > 0.05$, $^{*}P < 0.05$, $^{**}P < 0.01$, $^{***}P < 0.001$ compared with the DMSO group.

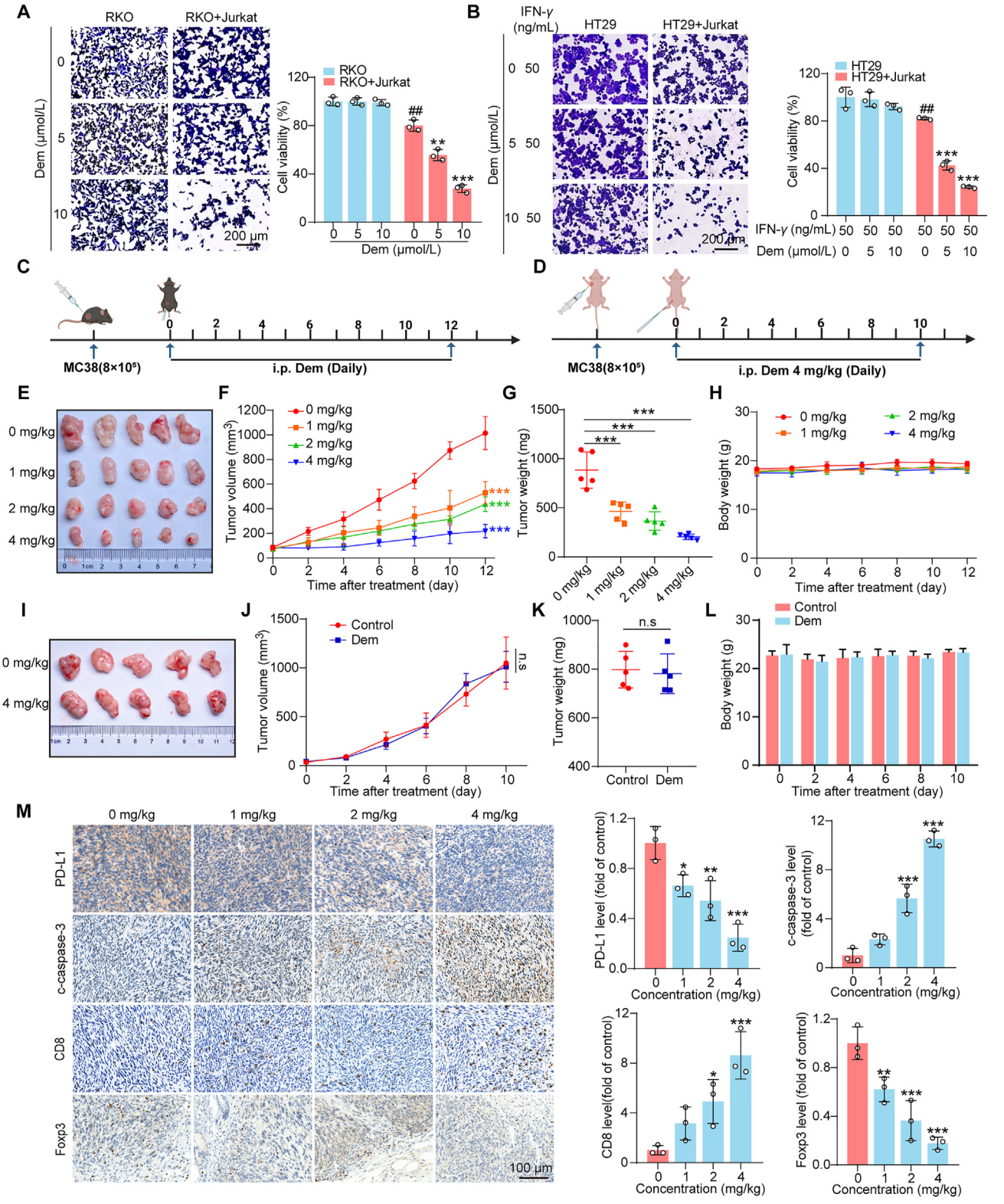

Figure 2 Dem can enhance the killing ability of T cells and inhibit tumor growth in mice with normal immune function *in vivo*. (A, B) Jurkat cells were activated with 1 mg/mL phytohemagglutinin (PHA) and 50 ng/mL phorbol 12-myristate 13-acetate (PMA) and cocultured with RKO and HT29 cells for 24 h in the presence of Dem. The surviving tumor cells were visualized by crystal violet staining. The quantitative results for the surviving cells are shown on the right ($n = 3$). $^{\#\#}P < 0.01$ compared with the RKO or HT29 DMSO group; $^{**}P < 0.01$ and $^{***}P < 0.001$ compared with the RKO + Jurkat cell or HT29+Jurkat cell group. Scale bar = 200 μm. A subcutaneous tumor model was constructed in C57BL/6 mice (C) or nude mice (D), and the process of drug administration was performed. (E−H) Effect of Dem (1, 2, or 4 mg/kg) treatment on tumor growth in C57BL/6 mice ($n = 5$). Tumors were harvested at the 12-day follow-up (E), tumor volume (F), tumor weight (G), and body weight (H). (I−L) Effect of Dem

study. Consistent with the Western blotting results, the flow cytometry results showed that Dem effectively inhibited PD-L1 expression on the cell membranes of RKO and HT29 cells (Fig. 1G−J). In addition to its effect on colorectal cancer cells, Dem also reduced the level of PD-L1 on the membrane of H460 and A549 lung cancer cells (Fig. S1D). Therefore, these results suggested that Dem has a certain broad effect on the degradation of PD-L1. Furthermore, the immunofluorescence results also showed that the fluorescence intensity of PD-L1 on the cell membrane was dramatically lower in the Dem-treated group than in the control group (Fig. 1K, L and Fig. S1G and S1H). In addition, EdU and CCK-8 experiments further confirmed that Dem had no significant cytotoxic effect on RKO or HT29 cells (Fig. 1M, N and Fig. S1E, S1F, S1I, S1J). In conclusion, Dem can significantly downregulate PD-L1 expression in CRC cells.

3.3. *Dem enhances the cytotoxicity of T cells*

When PD-L1 on tumor cells binds to the PD-1 receptor on the surface of T cells, T cells can transmit negative regulatory signals, thus inhibiting the recognition of cancer cells and promoting the immune escape of tumor cells[12]. Therefore, we explored whether Dem could improve the killing ability of T cells by reducing the expression of PD-L1 on the membrane surface of tumor cells. We cocultured PD-1-transfected Jurkat cells with RKO cells and HT29 cells and detected the surviving tumor cells using crystal violet staining[34]. As shown in Fig. 2A and B, Dem markedly reduced the survival of RKO and HT29 cells. To demonstrate that Dem exerts antitumor effects by reducing PD-L1, we established PD-L1-deficient cell models with PD-L1 interference in tumor cells *in vitro*. We knocked down PD-L1 using siRNA in RKO cells and then cocultured RKO cells with activated PD-1-transfected Jurkat cells. As shown in Supporting Information Fig. S2, we observed that knockdown of PD-L1 had effects similar to those of treatment with Dem alone, indicating that reducing PD-L1 enhances the ability of T cells to kill tumors. To further demonstrate whether Dem enhances T cell killing *in vitro* by reducing PD-L1, we combined Dem with si-PD-L1 and found that the results were almost consistent with those obtained with Dem alone or si-PD-L1. This finding suggested that Dem could not synergize with si-PD-L1, which further indicates that Dem enhances the killing ability of T cells only by reducing tumor cell PD-L1. These results suggested that Dem increased the cytotoxicity of T cells toward cancer cells by downregulating PD-L1 expression in cancer cells.

3.4. *Dem inhibits the growth of MC38 tumors in vivo by activating tumor-infiltrating T cells*

We next investigated whether Dem could inhibit tumor growth *in vivo*. MC38 cells were inoculated into C57BL/6 mice (Fig. 2C), after which the growth of the tumors was monitored. When the average tumor volume reached 50 mm^3, the mice were randomly divided into four groups and treated with Dem daily for 12 days. During the Dem administration period, we monitored the body weights and tumor volumes of the mice and recorded them every two days. Consistent with the *in vitro* results, intraperitoneal infusion of Dem dramatically reduced the volume and weight of subcutaneous tumors in mice compared with vehicle infusion (Fig. 2E−G). During administration, Dem did not significantly change the body weight of the mice (Fig. 2H). Consistent with the antitumor effect, immunohistochemistry (IHC) revealed that the levels of PD-L1, Foxp3, and Ki-67 were decreased in Dem-treated mice, while the levels of CD8 and cleaved caspase-3 were increased, suggesting that Dem induces significant apoptosis of mice tumor cells through activation of T cell immunity (Fig. 2M and Supporting Information Fig. S3A). Moreover, Dem did not cause systemic toxicity in mice, and there were no significant changes in the main organs of the treated mice (Supporting Information Fig. S4A). Overall, these results indicated that Dem significantly inhibited tumor growth and induced significant cell apoptosis *in vivo*, with no significant toxic side effects on the mice.

To prove that Dem has an antitumor impact by enhancing the killing capacity of T cells, we examined TILs in mice tumor tissues. We found that Dem treatment increased the release of GzmB when compared with the control treatment, indicating that Dem increased the activity of cytotoxic T cells. Additionally, the populations of $CD4^+$ $CD25^+$ $Foxp3^+$ and $CD11b^+$ $Gr\text{-}1^+$ cells, which are indicators of Tregs activation and MDSCs accumulation, respectively[35,36], were markedly suppressed after Dem treatment (Fig. S3B). These results demonstrated that Dem could effectively stimulate the activation of TILs by downregulating the expression of PD-L1 and activating the immune microenvironment, thus inhibiting the growth of subcutaneous tumors in mice. Interestingly, Dem failed to suppress the growth of MC38 tumors in nude mice with defective T cell function, indicating that Dem mediated antitumor activity by activating T cell immunity (Fig. 2D, I−L). Similarly, Dem in nude mice did not cause any significant toxic side effects (Fig. S4B). In conclusion, these findings demonstrated that Dem could enhance the killing capacity of T cells against cancer cells by downregulating the expression of PD-L1, thus exerting excellent antitumor effects both *in vitro* and *in vivo*.

3.5. *Dem promotes PD-L1 degradation via the ubiquitin-proteasome pathway*

To further clarify the mechanism by which PD-L1 is downregulated by Dem, we analyzed the mRNA levels of PD-L1 in RKO cells treated with Dem. Real-time PCR assays showed that Dem had no significant effect on PD-L1 mRNA expression (Fig. 3A and B). Moreover, treatment with Dem did not result in a significant change in the mRNA level of PD-L1 upon IFN-γ stimulation (Supporting Information Fig. S5A), suggesting that Dem did not regulate PD-L1 expression at the transcriptional level. We further confirmed these results by using the protein translation inhibitor CHX. As shown in Fig. 3C, Dem considerably reduced the protein half-life of PD-L1, suggesting that Dem is involved in regulating the expression of PD-L1 through post-translational mechanisms.

(4 mg/kg) treatment on tumor growth in nude mice ($n = 5$). Tumors were harvested at the 10-day follow-up (I), tumor volume (J), tumor weight (K), and body weight (L). (M) IHC staining results for PD-L1, c-caspase-3, CD8, and Foxp3. The quantitative results of IHC staining are shown on the right. Scale bar = 100 μm. The data shown are the mean ± standard error of the mean (SEM); n.s $P > 0.05$, $^*P < 0.05$, $^{**}P < 0.01$, and $^{***}P < 0.001$ compared with the saline group.

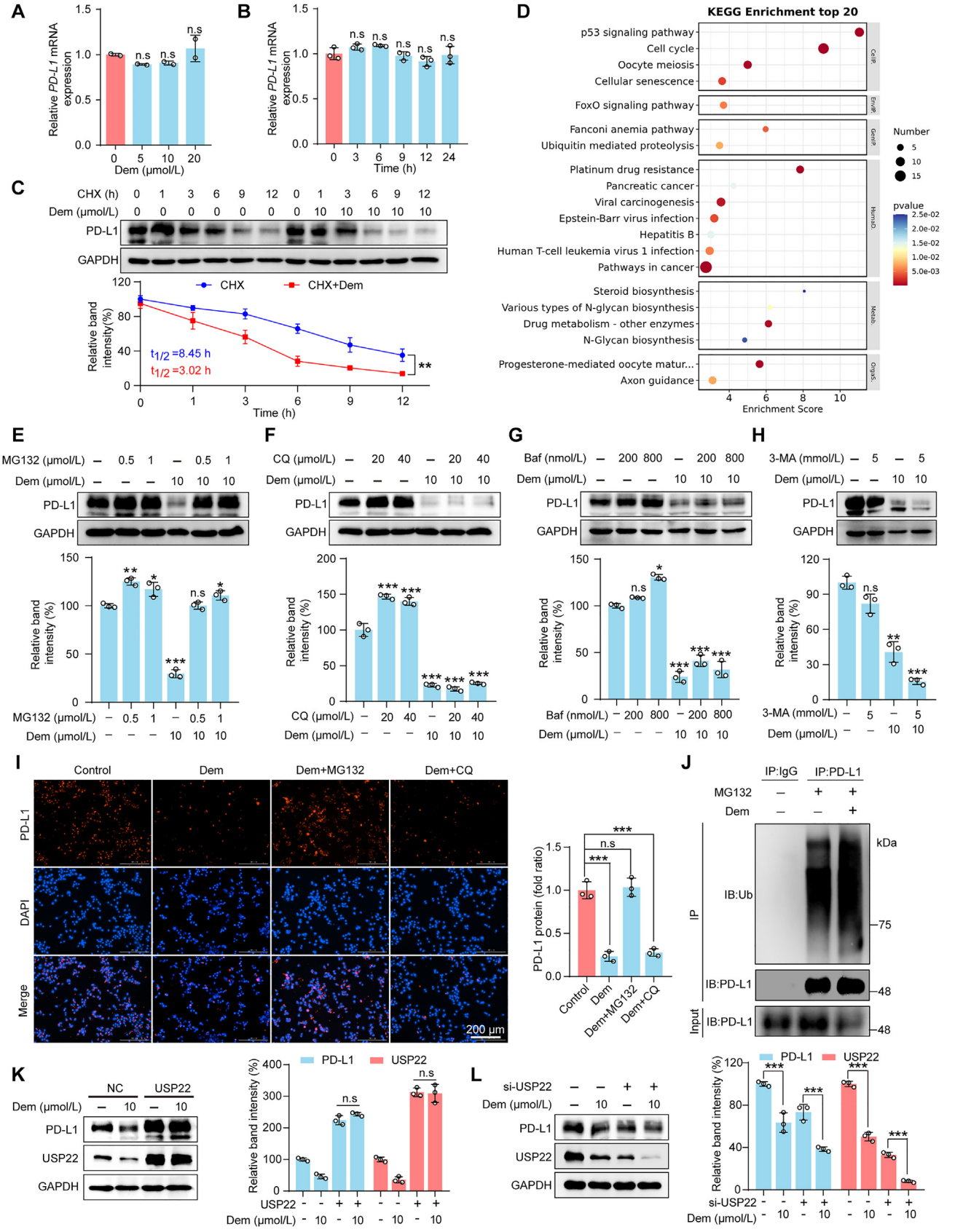

Figure 3 Dem promotes PD-L1 degradation *via* the ubiquitin/proteasome pathway. (A, B) Quantitative RT-PCR analysis of the mRNA level of PD-L1 in RKO cells treated with different concentrations of Dem for 24 h and treated with 10 μmol/L Dem for the indicated times. (C) IB analysis of PD-L1 levels in RKO cells treated with Dem or CHX (25 μg/mL) alone or in combination for the indicated durations. The quantitative results

According to previous reports, the degradation of the PD-L1 protein in eukaryotic cells mainly involves proteasome- and lysosomal-dependent degradation pathways[14,15]. Next, we investigated the pathway by which Dem promoted the degradation of the PD-L1 protein. First, we performed a proteomic analysis of RKO cells treated with Dem to identify signaling pathways potentially regulated by Dem. By conducting a KEGG pathway enrichment analysis of the proteomic data, we found that Dem likely activated the intracellular proteasome signaling pathway (Fig. 3D). Therefore, we used these inhibitors for further verification. The results showed that only the proteasome inhibitor MG132 was able to block the degradation of PD-L1 by Dem, whereas the lysosomal inhibitors CQ, Baf, and 3-MA were not able to (Fig. 3E−H). Moreover, the immunofluorescence staining results also showed that MG132 blocked Dem-induced PD-L1 degradation on RKO and HT29 cell membranes (Fig. 3I, Fig. S5B). In addition, the ubiquitination of PD-L1 was significantly increased after Dem treatment, as shown by endogenous immunoprecipitation (Fig. 3J). Taken together, these findings indicated that Dem promoted the degradation of PD-L1 through the ubiquitin-proteasome pathway.

3.6. *Dem directly binds to USP22 and promotes its degradation*

The E3 ligase can bind to the ubiquitin chain of the target protein, resulting in degradation by the 26S proteasome complex[10]. Studies have shown that the E3 ubiquitin ligases HRD1, BTRC, STUB1, ARIH1, SPOP, A20, and MARCH8 are capable of ubiquitinating PD-L1 and promoting its degradation[12-18]. We suspected that Dem might promote the degradation of PD-L1 through these E3 ubiquitin ligases. Therefore, we knocked down these ligases by using siRNA in RKO cells. However, the knockdown of the E3 ligase mentioned above did not reverse the degradation effect of Dem on PD-L1 (Fig. S5C−S5I). Therefore, we redirected our focus to deubiquitinating enzymes, which can efficiently remove ubiquitin from proteins and enhance the stability of the targeted substrate[37]. According to the literature, OTUB1, CSN5, and USP22 are all deubiquitinating enzymes of PD-L1 that can prolong its half-life and stabilize its expression[20,38,39]. We overexpressed these deubiquitinating enzymes in RKO cells and found that overexpression of OTUB1 or CSN5 had no irreversible effect on the degradation of PD-L1 induced by Dem (Fig. S5J and S5K). However, with the overexpression of USP22, the degradation of PD-L1 caused by Dem was dramatically reversed (Fig. 3K). As shown in Fig. 3L, we found that Dem significantly downregulated the protein expression of USP22 in RKO cells. Moreover, knocking down USP22 reduced the expression of PD-L1. Due to the high efficiency of USP22 degradation by Dem, Dem will continue to degrade the remaining USP22 protein, resulting in further degradation of PD-L1 levels.

To confirm whether Dem is directly bound to the USP22 protein, we conducted a cellular thermal shift assay (CETSA). This experiment was based on the principle that the binding of ligands to target proteins can improve the thermal stability of proteins and decrease the likelihood of denaturation compared with natural proteins at the same temperature. It is mainly used to verify the binding of drugs to target proteins[30,40]. We incubated the lysates with or without 100 μmol/L Dem for 5−10 min. Surprisingly, we found that Dem significantly promoted USP22 protein degradation at all temperatures, even at room temperature (Fig. 4A). Therefore, we incubated the lysates with 200 μmol/L Dem at room temperature for different durations. Consistent with the above results, Dem could degrade USP22 after 10 min, but no significant difference in USP22 expression occurred after prolonging the incubation time (Fig. 4B and C). We then incubated the lysate with various concentrations of Dem for 10 min at room temperature and found that Dem could bind to and destabilize USP22 *in vitro* (Fig. 4D and E). Moreover, Dem further accelerated the degradation of USP22 in the presence of proteolytic enzymes (Fig. 4F and G).

To further clarify the binding site of Dem on the USP22 protein, we simulated the binding mode of Dem through molecular docking using MOE (Molecular Operating Environment) software. The molecular simulation docking results showed that the possible binding sites for Dem and USP22 were Arg371 and His374 (Fig. 4H). To further clarify the binding sites of Dem and USP22, we constructed GFP-labeled wild-type, Arg371, and His374 mutant USP22 plasmids and transferred them into 293T cells for binding analysis *via* microscale thermophoresis (MST). Consistent with the above experimental results, Dem bound to wild-type USP22 with a binding constant of 5.92 μM (Fig. 4I). Mutations in the His374 site of the USP22 protein did not affect its binding to Dem (Fig. 4J). However, when the Arg371 site was mutated, the interaction between Dem and USP22 disappeared (Fig. 4K). These results suggested that the Arg371 site was the site at which Dem binds to USP22. In addition, we overexpressed wild-type and Arg371 mutant USP22 plasmid in 293T cells. Then, the cell lysates were extracted and incubated with different concentrations of Dem. As shown in Supporting Information Fig. S6A and S6B, consistent with previous results, Dem was able to bind to wild-type USP22 and degrade it. However, Dem did not promote the degradation of the USP22 protein with the Arg371 mutation. We also overexpressed the Arg371 mutant USP22 plasmid in RKO cells to evaluate whether Dem increases the killing effect on T cells through the Arg371 site. The results showed that in the group overexpressing the NC plasmid, Dem treatment relieved the immunosuppressive effect on tumor cells and enhanced the killing ability of T cells. However, when the Arg371 mutant USP22 plasmid was overexpressed, Dem no longer showed the ability to enhance the killing effect of Jurkat cells (Fig. S6C−S6E). These results further suggested that Dem exerts its degradation function

are shown below. (D) KEGG enrichment of the top 20 signaling pathways identified *via* proteomics. (E−H) IB analysis of PD-L1 levels in RKO cells treated with Dem in the absence or presence of the inhibitors MG132 (E), CQ (F), Baf (G), and 3-MA (H). The results of the quantitative IB analysis are shown below. (I) Immunofluorescence detection of PD-L1 expression on the cell membrane in RKO cells treated with Dem in the absence or presence of the inhibitor MG132 (1 μmol/L) or CQ (20 μmol/L). PD-L1 is labeled in red, and nuclei are labeled in blue with DAPI. The quantitative results are shown on the right side. Scale bar = 200 μm. (J) Ubiquitinated PD-L1 in RKO cells were immunoprecipitated (IP) and subjected to IB analysis with a ubiquitin antibody. The cells were pretreated with MG132 (10 μmol/L) for 6 h. (K) Expression of PD-L1 and USP22 after transfection of the USP22 plasmid into RKO cells. (L) Expression of PD-L1 and USP22 after transfection of USP22 interfering RNA into RKO cells. The quantitative results are shown on the right. The data shown are the mean ± standard error of the mean (SEM); $n = 3$; n.s $P > 0.05$, *$P < 0.05$, **$P < 0.01$, ***$P < 0.001$ compared with the DMSO group.

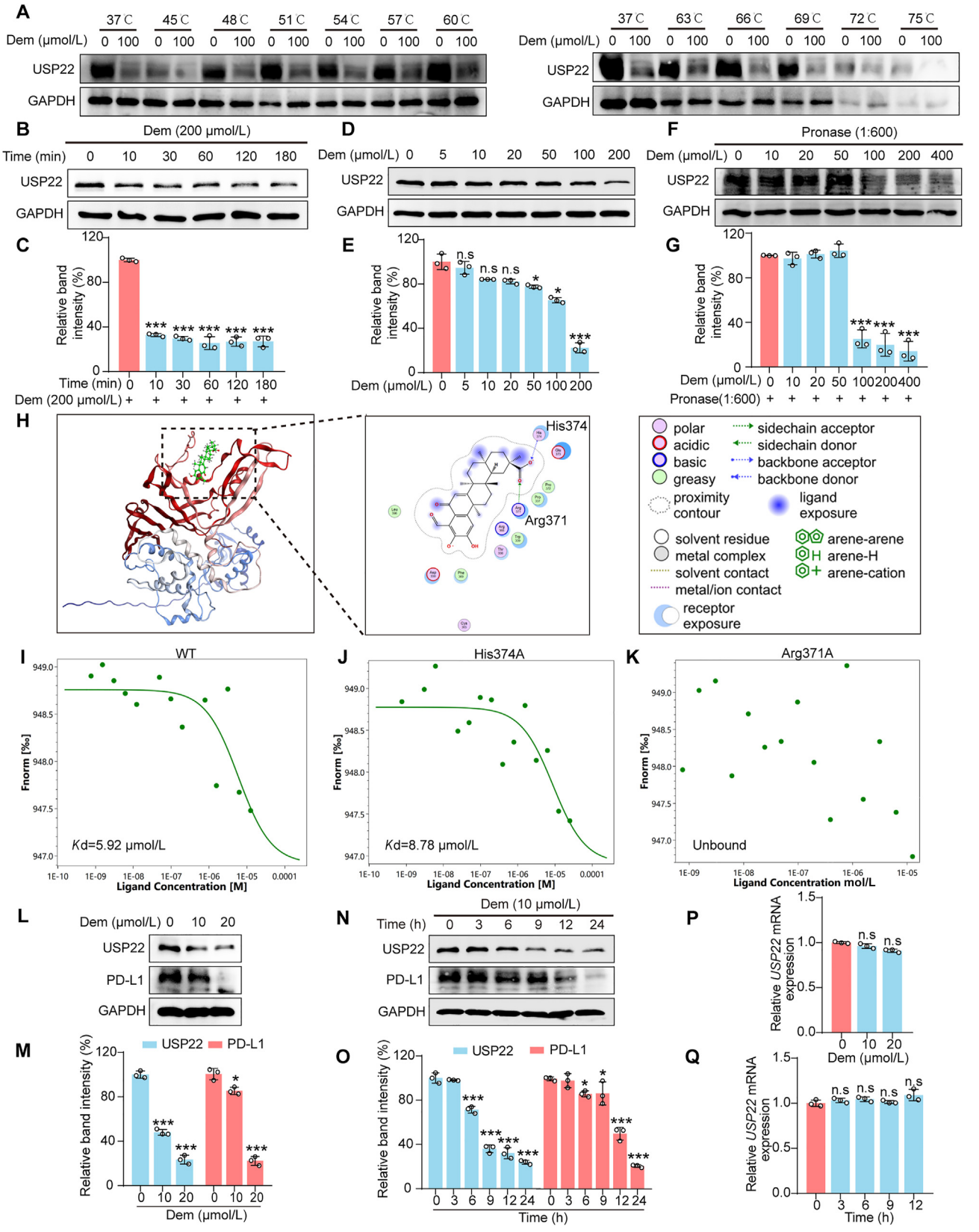

Figure 4 Dem binds to USP22 and promotes its degradation. (A) CETSA was used to determine the thermal instability of the interaction of USP22 with Dem at a series of temperatures ranging from 37 to 75 °C under short drug exposure (5 min). (B, C) CETSA was used to determine the thermal instability of the interaction of USP22 with Dem after different incubation times at room temperature. The quantitative results are shown below. (D, E) CETSA was used to determine the thermal instability of the interaction of USP22 with different concentrations of Dem at room temperature. The quantitative results are shown below. (F, G) The DARTS assay determined the instability of USP22 at different

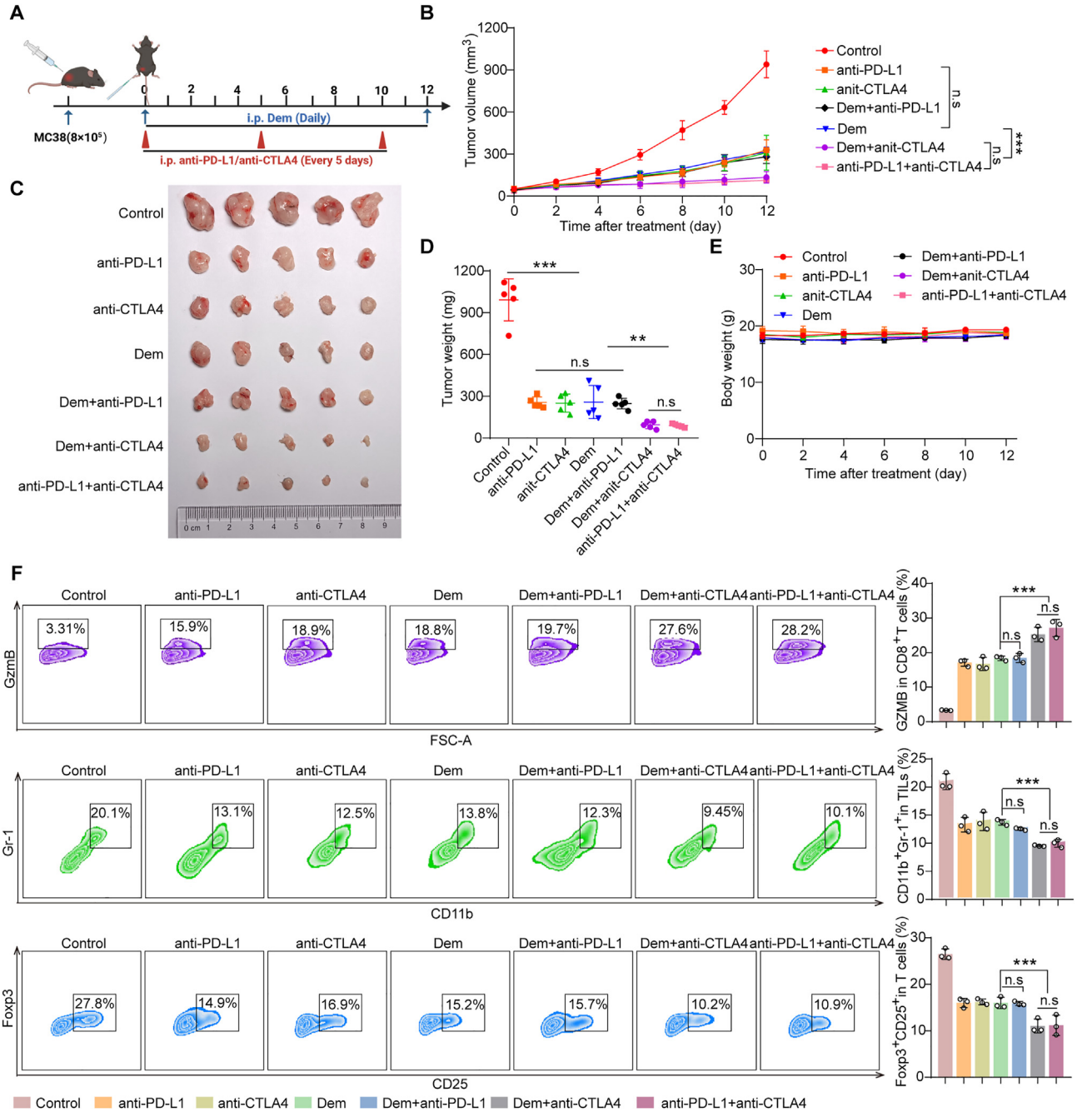

Figure 5 The combination of Dem and CTLA4 antibodies inhibits tumor growth in C57BL/6 mice. (A) Construction of a subcutaneous tumor model in C57BL/6 mice and the process of drug administration. (B−E) Effects of treatment with saline, anti-PD-L1, anti-CTLA4, Dem, Dem + anti-PD-L1, Dem + anti-CTLA4 or anti-PD-L1+anti-CTLA4 on tumor growth in C57BL/6 mice ($n = 5$). Tumor volume (B). Tumors were harvested at the 12-day follow-up (C). Tumor weight (D). Body weight (E). (F) Flow cytometry was used to detect GzmB$^+$, Gr-1$^+$ CD11b$^+$, and Foxp3$^+$ CD25$^+$ cells in these groups. The quantitative results of flow cytometry are shown on the right ($n = 3$). The data shown are the mean ± standard error of the mean (SEM); n.s $P > 0.05$, *$P < 0.05$, **$P < 0.01$, ***$P < 0.001$ compared with the saline group.

concentrations of Dem when the ratio of pronase to protein was 1:600. The quantitative results are shown below. (H) Molecular docking of Dem to USP22. (I−K) Cellular MST assay of GFP-tagged USP22 upon overexpression of wild-type USP22 (I) or disrupted USP22 mutants (Arg371 and His374) (J, K). (L−O) Immunoblot analysis of USP22 levels in RKO cells treated with different concentrations of Dem for 24 h and treated with 10 μmol/L Dem for the indicated times. The quantitative results are shown below. (P, Q) Quantitative RT-PCR analysis of the mRNA level of USP22 in RKO cells treated with different concentrations of Dem for 24 h (P) and treated with 10 μmol/L for the indicated times (Q). The data shown are the mean ± standard error of the mean (SEM); $n = 3$; n.s $P > 0.05$, *$P < 0.05$, **$P < 0.01$, ***$P < 0.001$ compared with the DMSO group.

by binding to the Arg371 site of USP22. Moreover, we also detected the impact of Dem on the intracellular expression of the USP22 protein. The results showed that Dem promoted the degradation of USP22 in a concentration- and time-dependent manner (Fig. 4L–O) and did not affect the mRNA level of USP22 (Fig. 4P and Q). Since USP22 is a deubiquitinating enzyme for PD-L1, we examined the effect of Dem on the deubiquitinating activity of USP22. The results of *in vitro* deubiquitination experiments showed that Dem had no significant inhibitory effect on the level of 7-amino-4-methylcoumarin (AMC), the fluorescent substrate of Ub hydrolase, indicating that Dem did not affect the deubiquitination activity of USP22 obviously (Fig. S6F). Taken together, these results suggested that Dem can directly bind to USP22 and promote its degradation.

3.7. The combination of Dem and CTLA4 blockade effectively suppressed tumor growth in vivo

It has been reported that combining PD-L1 antibodies and CTLA4 antibodies can not only enhance the antitumor immune response but also eliminate regulatory T cells and reduce the side effects of PD-L1 antibody therapy[41]. Next, we used a combination of CTLA4 antibody and Dem in an MC38 tumor model to explore whether this combination could achieve improved efficacy in mice. As shown in Supporting Information Fig. S7, compared with that in the control group, tumor growth was significantly inhibited in the treatment groups treated with Dem or anti-CTLA4 alone. Notably, the tumor growth rate, tumor volume, and tumor weight further improved after combination treatment with Dem and anti-CTLA4. In addition, there was no significant change in body weight or obvious toxicity or side effects in the experimental groups of mice (Fig. S7E, Supporting Information Fig. S8). To further evaluate whether Dem is equivalent to PD-L1 antibody treatment, we compared the effects of Dem and PD-L1 antibody treatment on tumor growth. We found that the therapeutic effects in the Dem, anti-PD-L1, and anti-CTLA4 treatment groups were similar. In addition, to verify whether Dem plays an antitumor role only by inhibiting the expression of PD-L1, we compared the efficacy of Dem treatment and Dem plus anti-PD-L1 treatment. The results showed that combined treatment with PD-L1 antibody did not further increase the therapeutic effect of Dem, indicating that Dem and PD-L1 antibody treatment had no synergistic effect. Moreover, the therapeutic effect of Dem plus anti-CTLA4 was almost the same as that of anti-PD-L1 plus anti-CTLA4, which showed the clinical application value of Dem (Fig. 5A–E). Flow cytometry analysis revealed that the combination of Dem and CTLA4 antibodies markedly increased the expression level of GzmB, confirming that cytotoxic T cell activity was increased. Furthermore, the populations of activated MDSCs ($CD11b^+$ $Gr\text{-}1^+$) and Tregs cells ($CD4^+$ $CD25^+$ $Foxp3^+$) were dramatically decreased in the Dem and anti-CTLA4 combination-treated groups (Fig. 5F), indicating that Dem shifted the immune microenvironment from the suppressed state to the activated state. To elucidate the immune cell changes in the tumor microenvironment after Dem administration, we also detected the level of dendritic cells (DCs), macrophage cells, specific B cells, and natural killer (NK) cells. By analyzing DCs, we found that the proportion of $CD11c^+$ MCH II^+ cells was significantly increased, indicating enhanced antigen presentation and the increased proportion of $CD8^+$ T cells showed that the immunosuppressive environment was greatly improved. On the other hand, we also detected macrophages in the immune microenvironment. After Dem treatment, the number of M1 macrophages significantly increased, indicating that Dem reduced tumor PD-L1 expression and relieved the immune suppression of T cells, but also polarized macrophages toward the M1 phenotype. The results for both NK cells and B cells also confirmed that Dem promoted antitumor immunity (Supporting Information Fig. S9). Consistent with the flow cytometric results, immunohistochemical staining revealed that, compared with those in the other treatment groups, the combined treatment group had significantly lower PD-L1, Foxp3, and Ki-67 expression and greater CD8 and c-caspase-3 expression in tumor tissues (Supporting Information Fig. S10). In summary, these results indicated that the combination of Dem and CTLA4 antibodies can exert better antitumor effects *in vivo*.

3.8. High expression of USP22 in colorectal cancer is negatively associated with antitumor immunity

To further explore the correlation between the expression of USP22 and PD-L1 in the tumor tissues of patients with colorectal cancer and the influence of these expression patterns on patient prognosis, we first analyzed the overall survival of patient samples from The Cancer Genome Atlas colorectal cancer database. The results showed that patients with high PD-L1 and USP22 expression levels had poor clinical prognosis, while those treated with PD-L1 antibodies had longer survival (Fig. 6A). In addition, based on The Cancer Genome Atlas database, we analyzed the relationship between the expression of PD-L1 and USP22 with immune cell infiltration in colon adenocarcinoma using TIMER2.0. The results indicated that the expression of PD-L1 and USP22 was negatively correlated with the infiltration of $CD8^+$ T cells but was positively correlated with the infiltration of Tregs in the tumor immune microenvironment (Fig. 6B). These results demonstrated that tumors with high PD-L1 and USP22 expression can inhibit the activation of T cells in the tumor immune microenvironment. Moreover, we compared the expression of PD-L1 and USP22 in paracancerous and cancerous tissues of colon cancer patients. As shown in Fig. 6C, the expression of PD-L1 and USP22 in cancerous tissues was greater than that in paracancerous tissues. Collectively, our results suggested that USP22 stabilized the expression of PD-L1 in tumor tissues.

4. Discussion

PD-1/PD-L1 immune checkpoint inhibitor therapy can exert a significant therapeutic effect by restoring the host's antitumor immunity and has revolutionized the treatment of advanced solid tumors[42,43]. Although PD-1/PD-L1 antibody therapy has shown good efficacy in clinical application, there are disadvantages, such as primary or acquired resistance, poor stability and compliance, and high cost[44], while small molecule inhibitors have inherent advantages in pharmacokinetics and pharmacodynamics and thus have realistic potential to improve therapeutic indicators[45]. Increasing evidence suggests that small molecule targeted PD-L1 degradation is an important modality for enhancing immune checkpoint therapy efficacy. Recently, a lower dose of TBM-1 was shown to induce nuclear translocation of TFEB by directly binding to and inactivating mTOR, thereby triggering lysosomal degradation of PD-L1. Moreover, the combination of TBM-1 and anti-CTLA4 therapy effectively enhances antitumor T cell immunity and reduces the immunosuppressive infiltration of MDSCs and Treg cells[46]. In addition, BBR is considered to directly bind to CSN5 and promote PD-L1 degradation through a

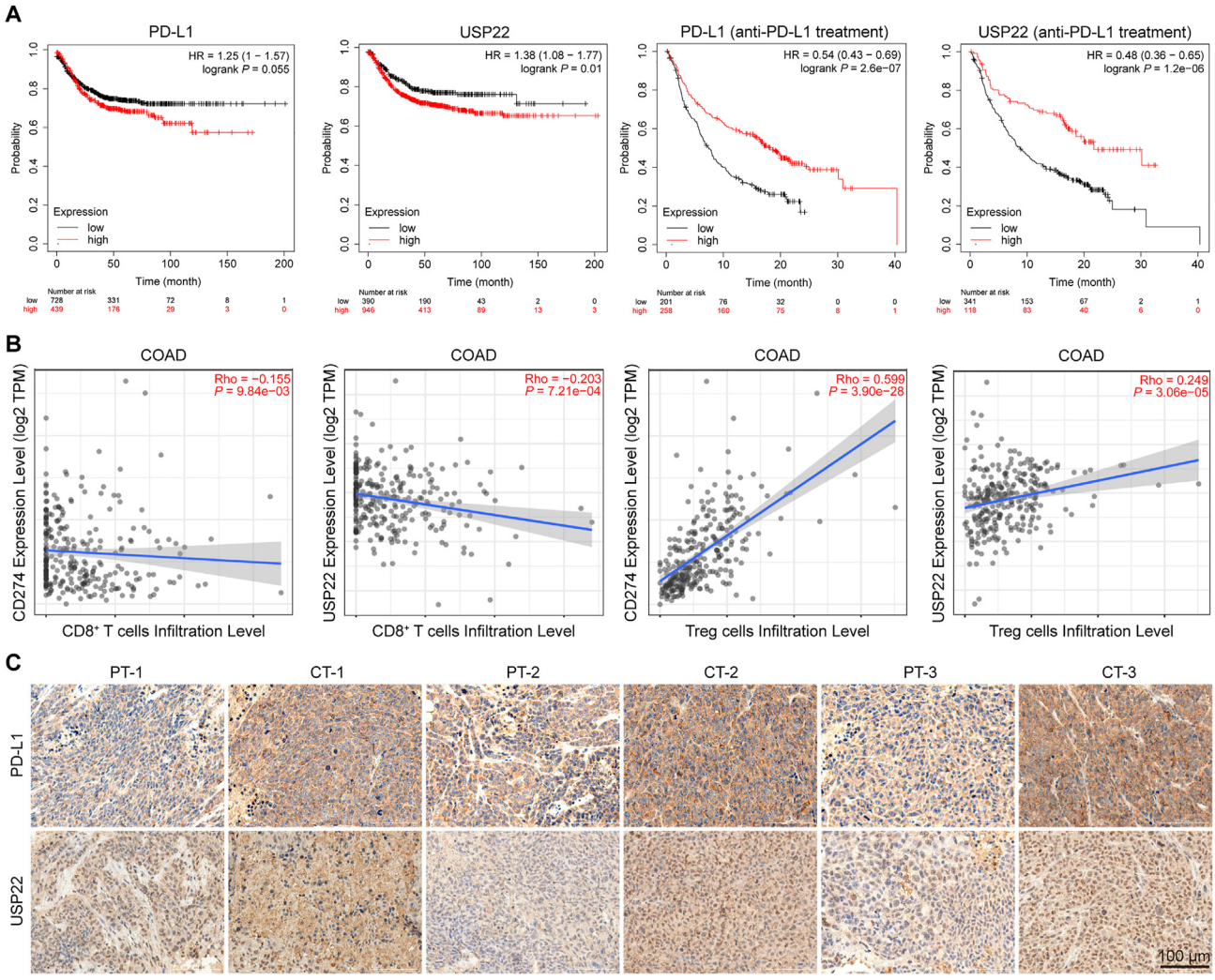

Figure 6 The association between PD-L1 and USP22 expression in CRC tissues. (A) The survival of CRC patients stratified by the expression of PD-L1 or USP22 was compared by two-side log-rank analysis. (B) Scatter plots showing the correlation between PD-L1 or USP22 expression and infiltrating $CD8^+$ T cells or Tregs in colon adenocarcinoma patients as determined by TIMER 2.0. (C) Representative IHC images of PD-L1 and USP22 staining in paracancerous tissues (PT) and cancer tissues (CT) from CRC patients. Scale bar = 100 μm.

ubiquitin (Ub)/proteasome-dependent pathway and to exert its antitumor effect in Lewis tumor xenograft mice by enhancing tumor-infiltrating T cell immunity[29]. In this study, through screening, we identified a small molecule called Dem, which can downregulate PD-L1 expression in colorectal cancer cells. Further mechanistic research confirmed that Dem directly targets USP22 and destabilizes it, leading to PD-L1 degradation and subsequent activation of tumor-infiltrating T cells, thereby inhibiting the progression of colorectal cancer. Here, we propose the potential of Dem as a small molecule inhibitor to disrupt PD-L1-mediated immunosuppression and preliminarily elucidate its mechanism.

It has been previously reported that Dem can inhibit the growth of melanoma and glioma cells[26,27]. We first evaluated the cytotoxicity of Dem against RKO and HT29 cells by CCK-8 and EdU experiments and found that treatment of colorectal cancer cells with 0−20 μmol/L Dem for 24 h did not result in significant cytotoxicity, indicating that Dem did not exert antitumor effects by affecting cell viability. Tumor cells suppress the activity of T cells through the high expression of PD-L1 on the cell surface, allowing them to evade T cell immune surveillance. To determine whether Dem inhibits tumor growth by regulating the tumor immune microenvironment, we cocultured PD-1-transfected Jurkat cells with RKO and HT29 cells and found that Dem significantly enhanced the killing effect of Jurkat cells on tumor cells. Moreover, *in vivo* experiments also showed that, compared with that in immunodeficient nude mice, Dem could significantly inhibit the growth of tumors in immunocompetent mice. Studies have indicated that MDSCs undergo massive expansion during tumor progression and inhibit the T-lymphocyte immune response, thereby protecting tumor cells from host immune attack[47]. Tregs suppress antitumor immune responses by directly interfering with the function of cytotoxic T cells[48]. In this study, flow cytometry revealed that the numbers of activated MDSCs and Tregs in TILs were significantly lower in the tumor tissues of Dem-treated mice than in those of control mice, indicating that Dem exerts antitumor immunity by activating TILs. Overall, our study suggested that Dem promotes antitumor T cell immunity by downregulating PD-L1.

CTLA4 is another checkpoint protein present on the surface of activated T cells. It competes with CD28 receptors and binds to B7-1 and B7-2 on antigen-presenting cells to inhibit T cell

activation[49]. Anti-PD-1/PD-L1 and anti-CTLA4 therapies play a role in different parts of the cancer immune cycle, and their combination can increase the response rate of patients[50]. In this study, we found that the combination of Dem and CTLA4 antibodies could inhibit the growth of tumors in mice to a greater extent than the use of antibodies alone, and the TILs in the tumor tissues of mice in the combined treatment group were further activated. This evidence indicates that Dem can help increase the effectiveness of tumor ICB therapy.

Ubiquitination is one of the most important types of post-translational modifications. E3 ubiquitin ligases and deubiquitinating enzymes play prominent roles in the occurrence and development of tumors[51]. In the present study, through proteomic analysis, we predicted that Dem may be involved in the regulation of ubiquitin-mediated protein degradation, which was further validated by inhibitors. Through screening E3 ligases and deubiquitinating enzymes that regulate PD-L1, it was found that overexpression of the deubiquitinating enzyme USP22 could block the degradation of PD-L1 by Dem. Currently, multiple studies have shown that USP22 is highly expressed in various solid tumors, such as lung cancer[52], melanoma[53], and colorectal cancer[54]. Increased USP22 expression is also associated with poor prognosis and metastasis in CRC patients[55,56]. Based on these findings, USP22 is considered a potential therapeutic target in colorectal cancer[57]. Previous studies have shown that USP22 promotes the stability of PD-L1 by directly deubiquitinating PD-L1 or by deubiquitinating CSN5[19,20], thereby promoting the surface expression of PD-L1 on tumor cells to evade immune monitoring[58]. Through CETSA and DARTS experiments, we demonstrated that Dem is directly bound to USP22. Unlike berberine, which promotes PD-L1 degradation by inhibiting the enzymatic activity of CSN5[29], Dem directly binds to USP22 and destabilizes it, which leads to PD-L1 degradation in turn. We predicted the site at which Dem binds to the USP22 protein by molecular docking and confirmed that the Arg371 site of the USP22 protein was the site at which Dem binds to the protein by MST. In addition, the results of proteomic experiments suggest that other signaling pathways or proteins, such as those involved in cellular senescence and human T cell leukemia virus 1 infection, may be involved in this regulation. However, whether there are other factors related to downregulating PD-L1 requires further exploration.

5. Conclusions

Our research demonstrated that Dem binds to the deubiquitinating enzyme USP22 and promotes its degradation, thereby increasing the ubiquitination of PD-L1 and causing its degradation through the proteasome pathway. The inhibitory effect of Dem on the PD-L1 protein can enhance T cell activity, promote T cell killing against cancer cells, and inhibit tumor growth *in vivo*. These findings suggest that Dem may be a promising compound for enhancing ICB therapy for colorectal cancer treatment.

Acknowledgments

This research was funded by the National Key Research and Development Program of China (2022YFC3502000), National Natural Science Foundation of China (Nos. 82141203, 82374086, and 82104459), Shanghai Municipal Science and Technology Major Project (ZD2021CY001, China), and Innovation Team and Talents Cultivation Program of National Administration of Traditional Chinese Medicine (ZYYCXTDD-202004, China), Science and Technology Commission of Shanghai Municipality (20YF1458700, China), Organizational Key Research and Development Program of Shanghai University of Traditional Chinese Medicine (2023YZZ02, China). We thank the staff members of the Large-scale Protein Preparation System at the National Facility for Protein Science in Shanghai (NFPS), Shanghai Advanced Research Institute, Chinese Academy of Science, China for providing technical support and assistance in data collection and analysis.

Author contributions

Yanyan Zhang: Writing − original draft, Investigation. Yun Huang: Validation, Investigation. Dianping Yu: Validation, Methodology. Mengting Xu: Validation, Methodology. Hongmei Hu: Validation, Methodology. Qing Zhang: Validation, Methodology. Minchen Cai: Validation, Methodology. Xiangxin Geng: Validation, Methodology. Hongwei Zhang: Validation, Methodology. Jianhua Xia: Validation, Methodology. Mengmeng Guo: Validation, Methodology. Dong Lu: Software, Methodology. Hanchi Xu: Validation, Methodology. Linyang Li: Validation, Methodology. Xing Zhang: Methodology. Qun Wang: Writing − review & editing, Supervision, Project administration, Methodology, Funding acquisition. Sanhong Liu: Writing − review & editing, Supervision, Project administration, Funding acquisition, Data curation, Conceptualization. Weidong Zhang: Writing − review & editing, Supervision, Project administration, Funding acquisition, Data curation, Conceptualization.

Conflicts of interest

The authors declare no potential conflicts of interest.

Appendix A. Supporting information

Supporting information to this article can be found online at https://doi.org/10.1016/j.apsb.2024.08.004.

References

1. Yamaguchi H, Hsu JM, Yang WH, Hung MC. Mechanisms regulating PD-L1 expression in cancers and associated opportunities for novel small-molecule therapeutics. *Nat Rev Clin Oncol* 2022;**19**:287−305.
2. Dong HD, Strome SE, Salomao DR, Tamura H, Hirano F, Flies DB, et al. Tumor-associated B7-H1 promotes T-cell apoptosis: a potential mechanism of immune evasion. *Nat Med* 2002;**8**:793−800.
3. Zou WP, Chen LP. Inhibitory B7-family molecules in the tumour microenvironment. *Nat Rev Immunol* 2008;**8**:467−77.
4. Inman BA, Longo TA, Ramalingam S, Harrison MR. Atezolizumab: a PD-L1-blocking antibody for bladder cancer. *Clin Cancer Res* 2017;**23**:1886−90.
5. Robert C, Schachter J, Long GV, Arance A, Grob JJ, Mortier L, et al. Pembrolizumab *versus* ipilimumab in advanced melanoma. *New Engl J Med* 2015;**372**:2521−32.
6. Yu XF, Li W, Liu HD, Wang X, Coarfa C, Cheng C, et al. PD-L1 translocation to the plasma membrane enables tumor immune evasion through MIB2 ubiquitination. *J Clin Invest* 2023;**133**:e160456.
7. Ren YM, Qian Y, Ai LY, Xie YL, Gao YQ, Zhuang ZY, et al. TRAPPC4 regulates the intracellular trafficking of PD-L1 and anti-tumor immunity. *Nat Commun* 2021;**12**:5405.

8. Mezzadra R, Sun C, Jae LT, Gomez-Eerland R, de Vries E, Wu W, et al. Identification of CMTM6 and CMTM4 as PD-L1 protein regulators. *Nature* 2017;**549**:106−10.
9. Hsu JM, Li CW, Lai YJ, Hung MC. Posttranslational modifications of PD-L1 and their applications in cancer therapy. *Cancer Res* 2018;**78**:6349−53.
10. Hou B, Chen T, Zhang H, Li JT, Wang PT, Shang GN. The E3 ubiquitin ligases regulate PD-1/PD-L1 protein levels in tumor microenvironment to improve immunotherapy. *Front Immunol* 2023;**14**:1123244.
11. Feng C, Zhang LN, Chang X, Qin DL, Zhang T. Regulation of post-translational modification of PD-L1 and advances in tumor immunotherapy. *Front Immunol* 2023;**14**:1230135.
12. Li CW, Lim SO, Xia WY, Lee HH, Chan LC, Kuo CW, et al. Glycosylation and stabilization of programmed death ligand-1 suppresses T-cell activity. *Nat Commun* 2016;**7**:12632.
13. Cha JH, Yang WH, Xia WY, Wei YK, Chan LC, Lim SO, et al. Metformin promotes antitumor immunity *via* endoplasmic-reticulum-associated degradation of PD-L1. *Mol Cell* 2018;**71**:606−20.
14. Burr ML, Sparbier CE, Chan YC, Williamson JC, Woods K, Beavis PA, et al. CMTM6 maintains the expression of PD-L1 and regulates anti-tumour immunity. *Nature* 2017;**549**:101−5.
15. Wu YQ, Zhang C, Liu XL, He ZF, Shan B, Zeng QX, et al. ARIH1 signaling promotes anti-tumor immunity by targeting PD-L1 for proteasomal degradation. *Nat Commun* 2021;**12**:2346.
16. Zhang JF, Bu X, Wang HZ, Zhu YS, Geng Y, Nihira NT, et al. Cyclin D-CDK4 kinase destabilizes PD-L1 *via* cullin 3-SPOP to control cancer immune surveillance. *Nature* 2018;**553**:91−5.
17. Zou JH, Xia HW, Zhang CL, Xu HJ, Tang QL, Zhu GM, et al. Casp8 acts through A20 to inhibit PD-L1 expression: the mechanism and its implication in immunotherapy. *Cancer Sci* 2021;**112**:2664−78.
18. Qian GQ, Guo JP, Vallega KA, Hu CJ, Chen Z, Deng YF, et al. Membrane-associated RING-CH 8 functions as a novel PD-L1 E3 ligase to mediate PD-L1 degradation induced by EGFR inhibitors. *Mol Cancer Res* 2021;**19**:1622−34.
19. Wang Y, Sun QG, Mu N, Sun XY, Wang YY, Fan SQ, et al. The deubiquitinase USP22 regulates PD-L1 degradation in human cancer cells. *Cell Commun Signal* 2020;**18**:112.
20. Huang X, Zhang Q, Lou Y, Wang JL, Zhao XY, Wang L, et al. USP22 deubiquitinates CD274 to suppress anticancer immunity. *Cancer Immunol Res* 2019;**7**:1580−90.
21. Feng TT, Ling SB, Xu CY, Ying LS, Su D, Xu X. Ubiquitin-specific peptidase 22 in cancer. *Cancer Lett* 2021;**514**:30−7.
22. Guo JH, Zhao J, Fu W, Xu QR, Huang DS. Immune evasion and drug resistance mediated by USP22 in cancer: novel targets and mechanisms. *Front Immunol* 2022;**13**:918314.
23. Kosinsky RL, Zerche M, Saul D, Wang X, Wohn L, Wegwitz F, et al. USP22 exerts tumor-suppressive functions in colorectal cancer by decreasing mTOR activity. *Cell Death Differ* 2020;**27**:1328−40.
24. Chen K, Guo WR, Li RX, Han YQ, Gao Q, Wang SZ. Demethylzeylasteral attenuates hepatic stellate cell activation and liver fibrosis by inhibiting AGAP2 mediated signaling. *Phytomedicine* 2022;**105**:154349.
25. Pan LH, Feng F, Wu JQ, Fan SB, Han JJ, Wang SX, et al. Demethylzeylasteral targets lactate by inhibiting histone lactylation to suppress the tumorigenicity of liver cancer stem cells. *Pharmacol Res* 2022;**181**:106270.
26. Zhao YZ, He J, Li J, Peng XZ, Wang XX, Dong Z, et al. Demethylzeylasteral inhibits cell proliferation and induces apoptosis through suppressing MCL1 in melanoma cells. *Cell Death Dis* 2017;**8**:e3133.
27. Zhang K, Fu G, Pan GZ, Li CY, Shen L, Hu RJ, et al. Demethylzeylasteral inhibits glioma growth by regulating the miR-30e-5p/MYBL2 axis. *Cell Death Dis* 2018;**9**:1035.
28. Wang LJ, Mei QJ, Xie Q, Li HY, Su P, Zhang L, et al. A comparative study of mesenchymal stem cells transplantation approach to antagonize age-associated ovarian hypofunction with consideration of safety and efficiency. *J Adv Res* 2022;**38**:245−59.
29. Liu Y, Liu XJ, Zhang N, Yin MX, Dong JW, Zeng QX, et al. Berberine diminishes cancer cell PD-L1 expression and facilitates antitumor immunity inhibiting the deubiquitination activity of CSN5. *Acta Pharm Sin B* 2020;**10**:2299−312.
30. Molina DM, Jafari R, Ignatushchenko M, Seki T, Larsson EA, Dan C, et al. Monitoring drug target engagement in cells and tissues using the cellular thermal shift assay. *Science* 2013;**341**:84−7.
31. Lomenick B, Hao R, Jonai N, Chin RM, Aghajan M, Warburton S, et al. Target identification using drug affinity responsive target stability (DARTS). *Proc Natl Acad Sci U S A* 2009;**106**:21984−9.
32. Xiao HM, Sun XH, Lin ZY, Yang Y, Zhang M, Xu ZC, et al. Gentiopicroside targets PAQR3 to activate the PI3K/AKT signaling pathway and ameliorate disordered glucose and lipid metabolism. *Acta Pharm Sin B* 2022;**12**:2887−904.
33. Xu ZR, Xu JQ, Sun SB, Lin W, Li YM, Lu QY, et al. Mecheliolide elicits ROS-mediated ERS driven immunogenic cell death in hepatocellular carcinoma. *Redox Biol* 2022;**54**:102351.
34. Yi M, Wu YZ, Niu MK, Zhu SL, Zhang J, Yan YX, et al. Anti-TGF-β/PD-L1 bispecific antibody promotes T cell infiltration and exhibits enhanced antitumor activity in triple-negative breast cancer. *J Immunother Cancer* 2022;**10**:e005543.
35. Wang J, Ke XY. The Four types of Tregs in malignant lymphomas. *J Hematol Oncol* 2011;**4**:50.
36. Sui HS, Dongye SY, Liu XC, Xu XH, Wang L, Jin CQ, et al. Immunotherapy of targeting MDSCs in tumor microenvironment. *Front Immunol* 2022;**13**:990463.
37. Altun M, Kramer HB, Willems LI, McDermott JL, Leach CA, Goldenberg SJ, et al. Activity-based chemical proteomics accelerates inhibitor development for deubiquitylating enzymes. *Chem Biol* 2011;**18**:1401−12.
38. Zhu D, Xu RD, Huang XP, Tang ZF, Tian YL, Zhang JF, et al. Deubiquitinating enzyme OTUB1 promotes cancer cell immunosuppression *via* preventing ER-associated degradation of immune checkpoint protein PD-L1. *Cell Death Differ* 2021;**28**:1773−89.
39. Lim SO, Li CW, Xia WY, Cha JH, Chan LC, Wu Y, et al. Deubiquitination and stabilization of PD-L1 by CSN5. *Cancer Cell* 2016;**30**:925−39.
40. Tu YB, Tan LH, Tao HX, Li YF, Liu HQ. CETSA and thermal proteome profiling strategies for target identification and drug discovery of natural products. *Phytomedicine* 2023;**116**:154862.
41. Zhang H, Dai ZY, Wu WT, Wang ZY, Zhang N, Zhang LY, et al. Regulatory mechanisms of immune checkpoints PD-L1 and CTLA-4 in cancer. *J Exp Clin Canc Res* 2021;**40**:184.
42. Motzer RJ, Tannir NM, McDermott DF, Frontera OA, Melichar B, Choueiri TK, et al. Nivolumab plus ipilimumab versus sunitinib in advanced renal-cell carcinoma. *New Engl J Med* 2018;**378**:1277−90.
43. Wolchok JD, Chiarion-Sileni V, Gonzalez R, Rutkowski P, Grob JJ, Cowey CL, et al. Overall survival with combined nivolumab and ipilimumab in advanced melanoma. *New Engl J Med* 2017;**377**:1345−56.
44. Kim JM, Chen DS. Immune escape to PD-L1/PD-1 blockade: seven steps to success (or failure). *Ann Oncol* 2016;**27**:1492−504.
45. Dhanak D, Edwards JP, Nguyen A, Tummino PJ. Small-molecule targets in immuno-oncology. *Cell Chem Biol* 2017;**24**:1148−60.
46. Liu XJ, Yin MX, Dong JW, Mao GX, Min WJ, Kuang ZA, et al. Tubeimoside-1 induces TFEB-dependent lysosomal degradation of PD-L1 and promotes antitumor immunity by targeting mTOR. *Acta Pharm Sin B* 2021;**11**:3134−49.
47. Li K, Shi HH, Zhang BX, Ou XJ, Ma QZ, Chen Y, et al. Myeloid-derived suppressor cells as immunosuppressive regulators and therapeutic targets in cancer. *Signal Transduct Tar* 2021;**6**:362.
48. Maharaj K, Uriepero A, Sahakian E, Pinilla-Ibarz J. Regulatory T cells (Tregs) in lymphoid malignancies and the impact of novel therapies. *Front Immunol* 2022;**13**:943354.
49. Mocellin S, Nitti D. CTLA-4 blockade and the renaissance of cancer immunotherapy. *Biochim Biophys Acta* 2013;**1836**:187−96.
50. Rotte A. Combination of CTLA-4 and PD-1 blockers for treatment of cancer. *J Exp Clin Canc Res* 2019;**38**:255.

51. Han SZ, Wang RK, Zhang YN, Li XY, Gan Y, Gao F, et al. The role of ubiquitination and deubiquitination in tumor invasion and metastasis. *Int J Biol Sci* 2022;**18**:2292−303.
52. Sun T, Zhang KQ, Li WD, Liu YZ, Pangeni RP, Li AM, et al. Transcription factor AP2 enhances malignancy of non-small cell lung cancer through upregulation of *USP22* gene expression. *Cell Commun Signal* 2022;**20**:147.
53. Li M, Xu Y, Liang J, Lin H, Qi X, Li F, et al. USP22 deficiency in melanoma mediates resistance to T cells through IFNγ−JAK1−-STAT1 signal axis. *Mol Ther* 2021;**29**:2108−20.
54. Jiang S, Song C, Gu X, Wang M, Miao D, Lv J, et al. Ubiquitin-Specific Peptidase 22 contributes to colorectal cancer stemness and chemoresistance *via* Wnt/β-Catenin pathway. *Cell Physiol Biochem* 2018;**46**:1412−22.
55. Liu YL, Yang YM, Xu H, Dong XS. Increased expression of ubiquitin-specific protease 22 can promote cancer progression and predict therapy failure in human colorectal cancer. *J Gastroen Hepatol* 2010; **25**:1800−5.
56. Liu YL, Yang YM, Xu H, Dong XS. Aberrant expression of USP22 is associated with liver metastasis and poor prognosis of colorectal cancer. *J Surg Oncol* 2011;**103**:283−9.
57. Melo-Cardenas J, Zhang YS, Zhang DD, Fang DY. Ubiquitin-specific peptidase 22 functions and its involvement in disease. *Oncotarget* 2016;**7**:44848−56.
58. Fan ZW, Wu CY, Chen MM, Jiang YY, Wu YY, Mao RF, et al. The generation of PD-L1 and PD-L2 in cancer cells: from nuclear chromatin reorganization to extracellular presentation. *Acta Pharm Sin B* 2022;**12**:1041−53.